Investigation on Radiation-Induced Latch-Ups in COTS SRAM Memories On-Board PROBA-V

André M P Mattos, Douglas A Santos, Lucas M Luza, Viyas Gupta, Thomas Borel, Luigi Dilillo

Title: Investigation on Radiation-Induced Latch-Ups in COTS SRAM Memories On-Board PROBA-V

Author(s): André M. P. Mattos, Douglas A. Santos, Lucas M. Luza, Viyas Gupta, Thomas Borel, and Luigi Dilillo

DOI: https://doi.org/10.1109/TNS.2024.3378668

Document version: Post-print version (Final draft)

Please cite the original version:
A. M. P. Mattos, D. A. Santos, L. M. Luza, V. Gupta, T. Borel and L. Dilillo, "Investigation on Radiation-Induced Latch-Ups in COTS SRAM Memories On-Board PROBA-V," in IEEE Transactions on Nuclear Science, doi: 10.1109/TNS.2024.3378668.

Investigation on Radiation-Induced Latch-Ups in COTS SRAM Memories On-Board PROBA-V

André M. P. Mattos, *Student Member, IEEE,* Douglas A. Santos, *Student Member, IEEE,* Lucas M. Luza, Viyas Gupta, Thomas Borel, and Luigi Dilillo, *Member, IEEE*

Abstract

This work investigates the flight behavior of Static Random-Access Memories (SRAMs) on board the PROBA-V satellite. During the mission, unexpected error rates were observed for redundant modules that used Commercial Off-The-Shelf (COTS) SRAMs. After undergoing an initial assessment, it was inferred that these errors were caused by Single-Event Latch-ups (SELs). This result led to a broader study on Single-Event Effects (SEEs) in these SRAM devices and their impact on the PROBA-V operation. Therefore, we proposed an experimental approach for evaluating and comparing the phenomena with the available PROBA-V flight data. Three experiments were performed: two irradiation campaigns, using heavy ions and protons, and laser testing. For that, a dedicated experimental setup was developed to enable the evaluation of specific test conditions and the discussion of hypotheses. The main results are reported, compared, and discussed. As an outcome of this study, we proposed an explanation for the observed behavior due to distinct environmental conditions of the redundant modules containing the SRAMs, notably temperature and satellite shielding.

Index Terms

SRAM, Radiation, SEL, SEE, Single-Event Effects, Flight Data, Memory, Heavy ions, Protons, Laser

I. Introduction

RELIABILITY in space applications is highly dependent on the radiation effects present in this harsh environment [1]. For satellites orbiting Earth, there are three main radiation sources: Galactic Cosmic Rays (GCRs), Solar Energetic Particles (SEPs), and trapped radiation [2, 3]. PROBA-V [4], Project for On-Board Autonomy (with V standing for vegetation), is a satellite in Low Earth Orbit (LEO) developed and launched by the European Space Agency (ESA). It introduced a miniaturized version of the VEGETATION instruments, specially designed to track the vegetation's evolution and its links to climate changes from the SPOT 4 and 5 satellites. PROBA-V was launched in May 2013 into a Sun-Synchronous Orbit (SSO) at an altitude of $820\ km$, and its main mission ended in June 2020. Although the satellite is still functional, the mission was ended due to the accumulation of orbital drift that impacted the consistency of the long-term data trends. Therefore, PROBA-V entered an experimental phase of operation, exploring other scientific interests.

During the mission, a module of PROBA-V presented an unexpected behavior. Despite being fully operational, the module had distinct error rates for redundant data buffer elements that are based on identical Commercial Off-The-Shelf (COTS) Static Random-Access Memories (SRAMs) protected by Error Correcting Code (ECC). The ECC is monitored and reported through telemetry data, enabling mission

This study has received funding from the European Union's Horizon 2020 research and innovation programme (grant agreement no. 101008126), from an ESA contract (contract no. 4000134557/21/NL/KML/rk), and from the Region d'Occitanie and the École Doctorale I2S from the University of Montpellier (contract no. 20007368/ALDOCT-000932).

A. M. P. Mattos, D. A. Santos, and L. Dilillo are with IES, University of Montpellier, CNRS, Montpellier, France. Contact: {andre.martins-pio-de-mattos, douglas.santos, luigi.dilillo}@umontpellier.fr.

L. M. Luza was with LIRMM, University of Montpellier, CNRS, Montpellier, France. He is now with SENAI Innovation Institute in Embedded Systems, Florianopolis-SC, 88054-700, Brazil. Contact: lucas.luza@sc.senai.br.

V. Gupta and T. Borel are with European Space Agency, ESTEC, 2200 AG Noordwijk, The Netherlands. Contact: Viyas.Gupta@esa.int, Thomas.Borel@ext.esa.int.

operators to understand and track the flight behavior. Due to this observability, the mission developers and operators were able to formulate hypotheses to explain the unexpected behavior and issue further investigations. For instance, a major inference was correlating Single-Event Latch-up (SEL) phenomena with some of the events observed in the early phases in orbit. In this context, we follow the efforts of these studies, leveraging flight data collected during the mission and providing experimental results needed to explain the satellite behavior.

In further detail, SEL is a type of Single-Event Effect (SEE), i.e., a radiation-induced phenomenon that affects electronic devices, notably memories, in the space environment [5, 6]. This event occurs when an ionizing particle affects a region of the transistor that results in a parasitic current, causing the current consumption of a device to significantly increase and potentially leading to a critical failure of the system [7, 8]. For representative radiation characterization (notably, SEL) targeting space environments, experimental investigation using proton and heavy-ion irradiation is a consolidated approach in the space community [9–11]. There are many strategies for SEL testing reported in the literature, ranging from simplified component screening [12, 13] to more elaborate characterization with dedicated equipment [14, 15]. Also, there are alternative use cases of laser testing for in-depth investigation of SEL phenomena, as explored in [16] and documented as guidelines in [17]. It is worth mentioning that understanding and mitigating SELs in COTS is very important for space projects since the new space philosophy is further pushing for the employment of COTS as part of reliable systems [18].

Therefore, this paper investigates the in-flight behavior observed for the PROBA-V SRAM devices, mainly targeting SELs, as part of a broader SEE study. For this purpose, we performed two irradiation experiments, using protons and heavy ions, and a laser testing campaign, for an in-depth analysis of the behavior observed during irradiation. The results are compared with the flight data acquired by PROBA-V, providing an insightful discussion and allowing initial hypotheses. Moreover, we briefly mention PROBA-II in-flight memory behavior, which used very similar SRAM devices, and SEL was also investigated.

The remainder of the paper is organized as follows. Section II introduces the studied SRAM memory, the SEL fault mechanism and model, and the observed in-flight behavior of these SRAMs. Section III details the proposed experimental analysis to investigate the behavior. Section IV presents the flight data, rate estimations based on the acquired experimental data, and an exploration of the hypotheses for the observed flight behavior. Then, Section V discusses the main outcomes of this study. Finally, Section VI concludes the paper.

II. Background

This section briefly introduces the studied SRAM, the latch-up phenomenon in SRAM memories, and details the behavior observed in these memories during the PROBA-V mission.

A. SRAM Description

The SRAM devices on-board PROBA-V were selected due to their flight heritage from different satellite missions, notably its predecessor PROBA-II [19–21]. However, due to procurement and component versioning issues, the expected SRAMs with part number *K6R4016V1C-TI10* (Rev. C) were erroneously replaced by the *K6R4016V1D-TI10* [22] (Rev. D). Both are COTS memories manufactured by Samsung with identical functional characteristics: a $4\ Mib$ SRAM with a 16-bit parallel interface. Despite the similarities, as later reported, the Rev. D presented higher sensitivity to radiation effects than the characterized and validated Rev. C. Therefore, in this study, we investigate the Rev. D, which is on-board PROBA-V, using two distinct manufacturing lots (*DC532* and *DC419*), including those from the same lot as the devices on-board PROBA-V for better phenomena correlation. Fig. 1 presents the delidded SRAM memory under analysis, in which the internal structures and die marking are visible.

B. Latch-up in SRAM Devices

An SRAM cell is generally composed of six transistors implemented in CMOS technology. Each cell stores a bit since it has two stable states that denote high and low logical levels. The CMOS technology

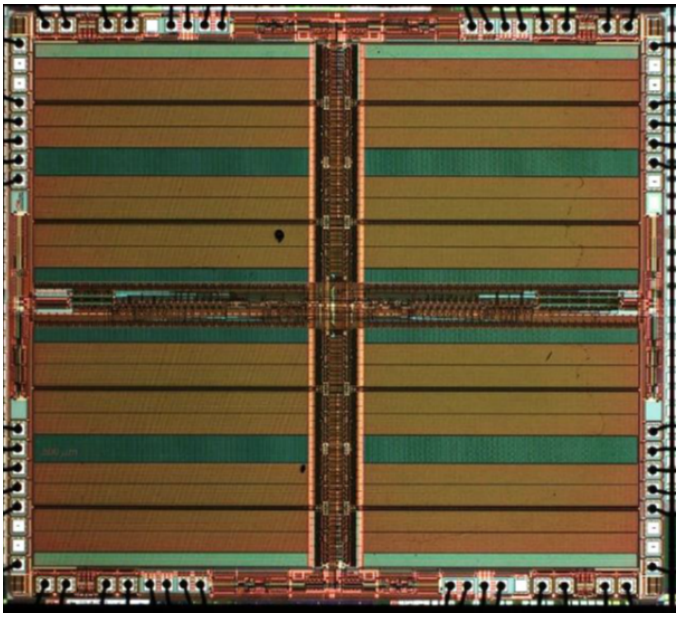

(a) Memory die stack.

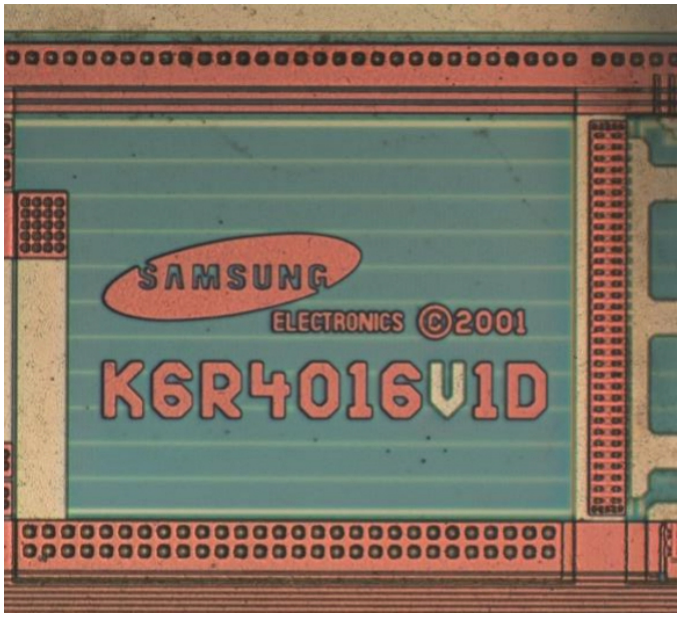

(b) Memory die mark.

Fig. 1. Delidded SRAM memory.

is susceptible to latch-ups due to a structure known as a thyristor, which nominally is in a high-impedance state. The SEL, a radiation-induced latch-up, occurs when this parasitic structure is affected by an ionizing particle interaction. In this event, the thyristor can enter a conducting state, generating a high-current state in the cell [7, 8], with consequent cell content loss. However, if a power cycle is quickly performed, this high-current state is suppressed, and the device may restore its nominal operation (besides the loss of data). When this occurs, the event is defined as a non-destructive SEL, in which permanent damage in the cell due to thermal runaway is avoided.

C. SRAMs in PROBA-V

In PROBA-V, these memories are located on the Mass Memory Unit (MMU) board of the Advanced Data and Power Management System (ADPMS). They are used as buffers to store the payload data on the mass memories of the satellite. There are two redundant MMU lines in distinct positions of the satellite, each having two SRAM memories. When an event requiring a power cycle occurs, such as an SEL, an automatic procedure was defined to switch between the redundant lines, i.e., data is transferred to the redundant line, which stores it for a brief period, allowing the primary line to be power cycled, and then the data is restored from the redundant line. This procedure takes about 3 to 4 minutes to complete.

Each memory was protected with ECC, which was also used to report the events. They are classified into two types of event flags and reported as part of the satellite housekeeping telemetry: *type 406*, correlated with ECC failure (uncorrectable errors); and *type 369*, when more than 1000 single ECC upsets are detected, but the memory remains fully operational. Whenever an error occurs related to a particular flag type, it is timestamped. During the mission, many errors classified as *type 406* were detected, possibly indicating radiation-induced latch-ups. This assumption was made during the initial phases of the satellite when current information on these memories was available, and a correlation was seen between SEL and ECC failures. It is worth mentioning that these devices were experimentally characterized prior to the mission, but the provided information gave insufficient insights to understand the flight behavior.

III. Experimental Analysis

The methodology in this work is based on performing experimental irradiation test campaigns to evaluate the SRAM memories and compare them with the observed flight behavior. In this section, we present and analyze the results from the experimental campaigns and the flight data.

A. Experimental Setup

We performed experiments in two irradiation facilities with different particles, heavy ions and protons, and with laser stimulation. Similar to [14], we created a dedicated experimental setup for testing the SRAMs. The architecture of this equipment is presented in Fig. 2. It consists of a controlling board, hosting an FPGA, and a test board, where the SRAM and measuring components were included. To allow handling current variations, we included power switches that were disabled at 50 ms (hold time) after an SEL event, allowing monitoring of the initial behavior under SEL and protecting the circuit from unrecoverable damage, and enabled again after 200 ms (cut time) to continue the test execution. These hold and cut time values were selected for consistency with previous characterizations. The data acquisition, handled by the controller, was made through a serial interface connected to a host computer. For current measurements, we used dedicated digital current sensors, which allowed precise measuring and a convenient interface with the controller. It is worth mentioning that the controller was implemented in a flash-based FPGA, in which the configuration memory is more robust to radiation effects [23], and the design included Triple Modular Redundancy (TMR) in the most critical elements to ensure proper operation during the tests. Hence, the controlling loop used the test algorithms and current monitoring to define the execution throughout the experiment and trigger the SEL protection and reporting.

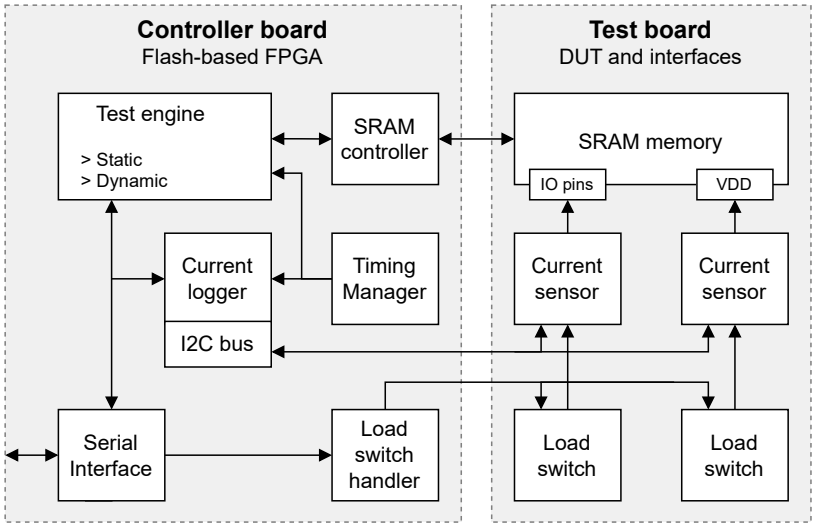

Fig. 2. Simplified diagram of the experimental setup used for the three experiments. The instrument is connected to a host computer through the serial interfaces.

This setup was proposed to allow flexibility, precise and coherent measurements, and representative test stimuli (e.g., static and dynamic test modes) for the targeted radiation facilities following the available testing standards [9, 17]. Since the experiments focus on SEL characterization, we designed a test board where current monitoring is done in the memory supply line and the IO banks. With the controlling board simultaneously managing these measurements and the test algorithms, it allowed coherent time stamping between both events, i.e., current variations and detected bit upsets. We applied the highest supply voltage within the nominal range for all tests. Using static and dynamic test modes supported a more representative radiation characterization by providing evaluation scenarios with data retention in low memory usage and realistically stressed cells, respectively. Thus, four test modes were used: 1. standby, when no operations

are performed (IOs in high impedance) and the device remains powered on; 2. chip-enabled, similar to the standby, except that the memory chip-select is set; 3. static, the memory is written using an alternated data background (0xAAAA), then, after a sufficient period, it is read back and checked with the same background; 4. dynamic, in which the memory is constantly written and read with different patterns (notably, March C- and Dynamic Stress algorithms [24, 25]), and errors are reported when detected.

For the heavy-ion experiment, eight SRAM devices were evaluated, covering the two manufacturing lots previously mentioned, and they required delidding for proper particle penetration. It allowed verifying the die markings and some internal structures, but unfortunately, some of the devices were compromised during the process and removed from the analysis. Various irradiation angles and test modes were explored in the heavy-ion campaign. Each test run was performed with a target fluence of up to $1 \times 10^7\ ions/cm^2$ unless a large number of SEL occurred beforehand (hundreds). For the proton experiment, four SRAM devices were used, of which two were reused from the previous experiment for better lot correlation, and two were pristine to avoid cumulative effect biases. Only the most relevant test modes were applied in this campaign, based on the outcomes from the heavy-ion experiments. The test runs for each test mode and beam energy targeted $1 \times 10^{11}\ p/cm^2$, reaching approximately $1 \times 10^{12}\ p/cm^2$ per Device Under Test (DUT). For the laser testing, the SEL identification is based on the same SEL monitoring system. However, a minor adaptation was implemented to enable integration with the facility monitoring equipment. An output signal was added to trigger an external event based on the current value and threshold. Then, it can combine the laser information (e.g., positioning, energy) with the SEL data provided by the test setup. The laser tests used two SRAM devices, delidded from the backside. The delidding was performed from the backside to avoid the metallization layers that would affect the desired laser properties in the case of front-side delidding. The laser test runs were defined based on the device sensitivity to each tested energy and temperature.

B. Heavy-Ion Irradiation

The Radiation Effects Facility (RADEF) at the University of Jyväskylä, Finland, was used for irradiation with heavy ions inside a vacuum chamber. The beam has a 10% homogeneity for the selected irradiation area and a heavy-ion cocktail of $16.3\ MeV/n$, capable of generating a flux up to approximately $3 \times 10^5\ ions/cm^2/s$. The ion selection is described in Table I, presenting the ion species and their respective energy, LET, and penetration range at the silicon surface in vacuum mode.

TABLE I
SELECTION OF ION SPECIES USED FOR THE HEAVY-ION TEST CAMPAIGN.

Ion Species	Energy [MeV]	LET [$MeVcm^2/mg$]	Range [μm]
$^{17}O^{6+}$	284	1.52	481
$^{40}Ar^{14+}$	657	7.2	264
$^{57}Fe^{20+}$	941	13.3	214
$^{83}Kr^{29+}$	1358	24.5	185
$^{126}Xe^{44+}$	2059	48.5	157

Fig. 3 presents the estimated SEL cross sections for the experiment with heavy ions. These cross sections were obtained by combining all the test modes due to the similar SEL responses: standby, chip-enabled, static, and dynamic. Some LETs were introduced by changing the DUTs angle in relation to the beam irradiation and are indicated as empty squares on the graph (instead of the solid squares). The error bars represent a 95% confidence interval with a 10% beam fluence uncertainty. Based on these cross sections, we did a Weibull fit using OMERE version 5.3 built-in algorithm, in which we excluded the LETs lower than $7.2\ MeVcm^2/mg$. The subsequent Weibull curve fittings used the same tool. Despite the reasonable capabilities of demonstrating the cross section trend for higher energies, the Weibull did not fit the lower LETs. In the literature, other researchers observe similar trends, in which the cross sections

for lower LETs suggest the superposition of effects or other physical interaction between the device and the incident particles [6, 26, 27]. We explored this phenomenon with the support of laser testing, which indicated additional possibilities. An important outcome of this test was that we did not observe significant part variability within the tested DUTs nor with previous characterization results, which was an initial assumption before the test.

Moreover, to evaluate possible biases in the SEE analysis due to accumulated doses, we assessed the SEL cross section with periodic intervals for multiple runs to observe their trends in relation to dose accumulation. This verification was possible due to the various beam configurations used (e.g., LET, angle of incidence) in distinct dose intervals. In summary, the DUTs accumulated dose (in silicon) ranged from $20\ krad$ to $32.4\ krad$ after irradiation, presenting no significant impact on the cross sections.

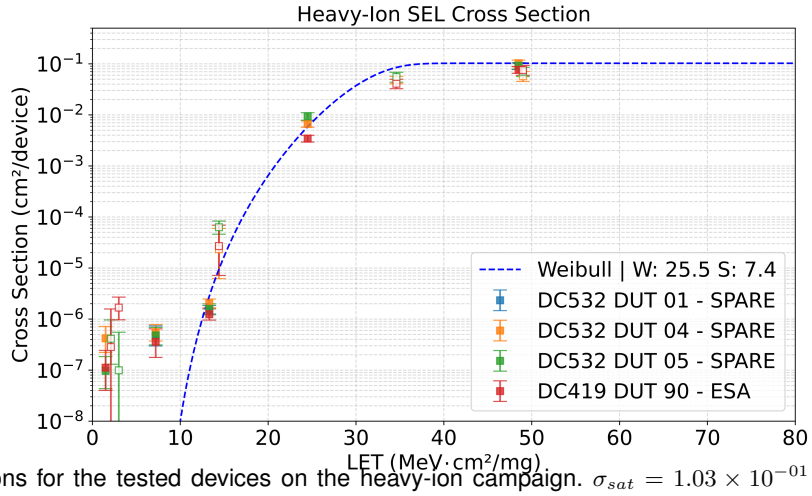

Fig. 3. SEL cross sections for the tested devices on the heavy-ion campaign. $\sigma_{sat} = 1.03 \times 10^{-01}\ cm^2/device$ and $LET_{th} = 7.2\ MeVcm^2/mg$. Test modes included standby, chip-enabled, static, March C-, and Dynamic Stress.

During the execution of dynamic tests, the occurrence of SELs caused sudden increases in the number of upsets in memory cells. Fig. 4 presents an example of an SEL increasing the error rate. It is noticeable that before it happened, the current consumption of the memory during each dynamic operation follows a pattern, and right after the SEL occurs by significantly increasing the current, the error rate also suddenly increases. This example is just one of the many SELs that also caused significant error rates to increase, and they were the typical behavior occurring in more than 95% of the events.

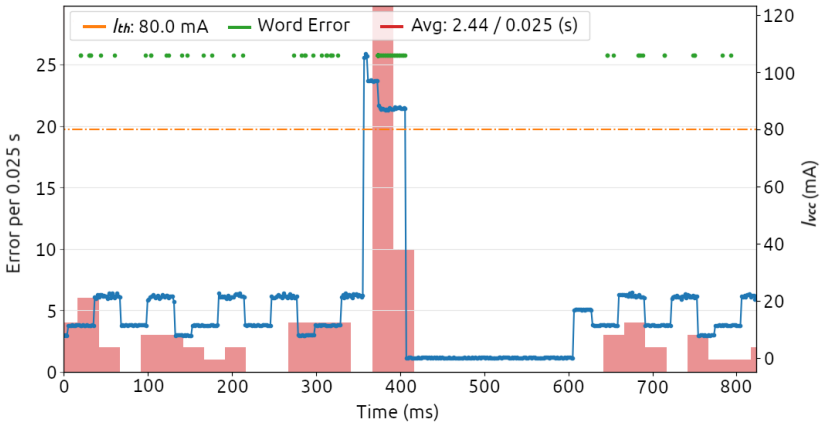

Fig. 4. Example of error rate (bit upsets) variation during SEL events. Test run for a dynamic test (March C-) during heavy-ion irradiation with a $LET = 14.4\ MeVcm^2/mg$.

Considering this correlation, we extended the analysis by generating logical bitmaps for each run to classify and distinguish these bit upsets during and outside SEL events. The logical bitmap is a

two-dimensional plot of the memory indexing contiguous data addresses following rows, columns, and arrays logical mapping. The bit upsets are plotted using the available timestamp to distinguish different events. Fig. 5 presents an example for this analysis using a test run with $48.5\ MeVcm^2/mg$ in dynamic mode (March C-). Besides the higher quantity of bit upsets during SEL events, they form column blocks in the logical bitmap. These block errors could surpass common mitigation schemes. Based on these characteristics, we classified each column block during SELs as a Single-Event Functional Interrupt (SEFI) and the isolated bit upsets as Single-Event Upsets (SEUs).

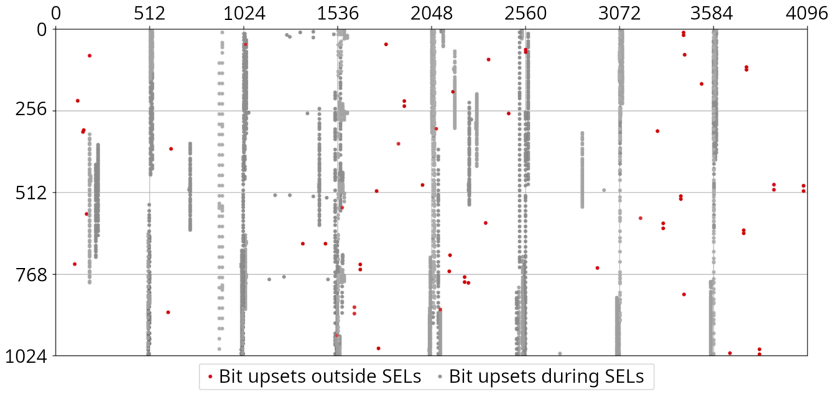

Fig. 5. Logical bitmap of the memory address space with the identified bit upsets during a March C- run with a LET of $48.5\ MeVcm^2/mg$. The *x* and *y* axis represent addresses in an arrangement based on the logical memory organization. For this bitmap, bit upsets during and outside SELs were highlighted in grayscale shades (for distinct events) and red, respectively.

C. Proton Irradiation

The Proton Irradiation Facility (PIF) at the Paul Scherrer Institute (PSI), Switzerland, was used for proton irradiation. According to the energy range suggested in [9], we selected the following proton energies for testing: 16, 29, 51, 70, 101, 151, and $200\ MeV$. Copper plates were introduced in the beam path to generate different energies, and two primary proton energies were used to allow proper testing at the lower energy range: 100 and $200\ MeV$. Proton fluxes of about 3×10^7 to $8 \times 10^7\ p/cm^2/s$ were used, and all tests were performed at ambient room temperature and air pressure. The beam had a 10% homogeneity for the selected irradiation area and beam energies throughout the full experiment. For this experiment, the accumulated fluence was $4.33 \times 10^{12}\ p/cm^2$, considering all DUTs and test modes.

Fig. 6 presents the estimated cross sections for the proton experiment. For protons with $16\ MeV$ and $29\ MeV$, no latch-up events were observed, so they are not presented in the graph. The DUTs 90 and 04 were reused from the previous experiment with heavy ions, so they already had some accumulated dose, and the DUTs 07 and 08 are memories that were never irradiated before this experiment. Based on the obtained results, no significant nor consistent differences were observed on the cross sections for these devices, suggesting that the accumulated dose for the tested ranges did not substantially impact the SEL response. Thus, the cross sections were combined to determine the Weibull parameters in the figure. The error bars represent a 95% confidence interval with a 10% beam fluence uncertainty.

It is worth mentioning that, in recent SRAM technologies, researchers have observed a significant SEE contribution of direct ionization caused by low-energy protons [28, 29]. However, these studies apply to deep submicron SRAMs (up to $90\ nm$), which is unlikely for the DUT in this work since it uses a relatively older technology node manufactured in 2001 or earlier. Furthermore, for the PROBA-V orbit (SSO at $820\ km$), the flux of low-energy protons is expected to be reduced (a few orders of magnitude) by the satellite's shielding. In [30], the impact of shielding is estimated for a similar orbit (SSO at $705\ km$), in which the contributions for the accumulated proton fluence are highly dependent on the proton energy itself. Considering the lowest tested energy in the proton experiment ($16\ MeV$), there is a fluence reduction of approximately ten times, reaching up to 5 orders of magnitude for low energies (few KeV) when considering

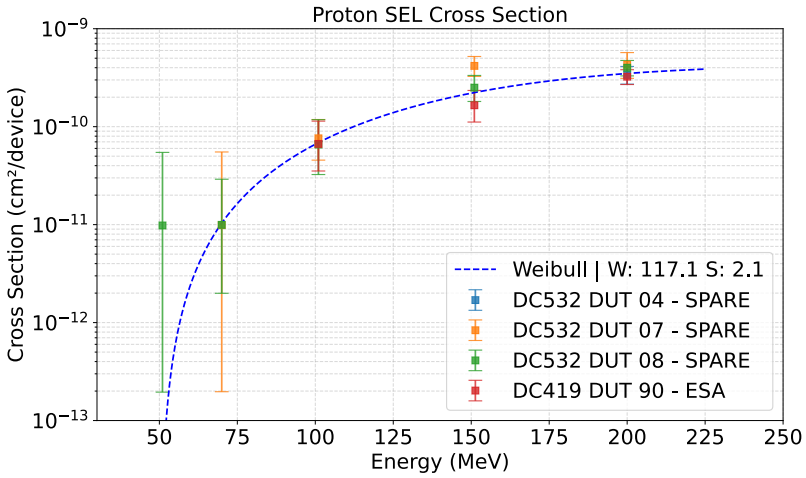

Fig. 6. SEL cross sections for the tested devices on the proton campaign. $\sigma_{sat} = 4.29 \times 10^{-10}\ cm^2/device$ and $E_{th} = 50.9\ MeV$. Test modes included static and March C-.

a $2.1\ cm$ aluminum shielding. Thus, given this significant fluence reduction and the observed SEL count for $16\ MeV$, only a minor impact is expected due to low-energy protons.

D. Laser Testing

The laser testing was performed at ESTEC, ESA, Netherlands. This facility uses the PULSYS-RAD (from PULSCAN) equipment, which is optimized for SEE testing. In particular, we used the PULSBOX Pico for this experiment, which uses picosecond laser stimulation and fault injection techniques. The generated laser uses the Single-Photon Absorption (SPA) technique with a wavelength of $1064\ nm$ and a temporal pulsewidth of $30\ ps$. The focused spot size is approximately $1.2\ \mu m$ with focusing optics of $\times 100$. The laser pulse rate was lower than $10\ Hz$. The applied scanning method consisted of a standard mapping, in which the laser moves in a grid pattern and is activated at defined points. For each laser activation, the DUT response was acquired. The tested energies reached up to $550\ pJ$ with horizontal and vertical step precision of $2\ \mu m$ and $4\ \mu m$, respectively, in the memory plane.

We started the laser testing campaign with preliminary assessments to understand important test parameters, such as latch-up sensitivity, affected areas, and latch-up current signatures. After this, tests were performed to evaluate the latch-up dependency on energy and device region. For that, the laser beam was configured with steps of $2\ \mu m \times 4\ \mu m$, capturing an SEL event related to each location depending on current behavior. The current level is set as the highest current observed in the active interval of the laser in the area. For energy dependency analysis, the current levels were represented with different colors for each area in a physical representation of the memory array using the $2\ \mu m \times 4\ \mu m$ areas as the base unit. The colors range from blue to red as the current increases, leaving the red colors for currents above the defined threshold. For the region dependency, zones were defined in specific regions of the device: memory array, internal controlling spines, and periphery in the edges. Fig. 7 presents the defined zones and a run executed to identify the general SEL sensitivity of an entire memory region. From that, it is possible to observe that the internal controlling spines and periphery in the edges did not contribute to the SEL occurrence for the tested laser energy. To report the laser cross sections, we calculated by multiplying the number of detected SEL events with the focused sensitive areas ($2\ \mu m \times 4\ \mu m$) expected for the entire memory die, as defined in [17].

Besides that, we observed two very distinct sensitivities for different regions, denoted as lower and higher energy effects. This notation was used due to the results of the heavy-ion experiment, in which the cross sections were higher than expected for lower LETs. Fig. 8 presents the SEL cross sections for the two regions highlighted in the bottom right quadrant in Fig. 7, using the same colors (green and

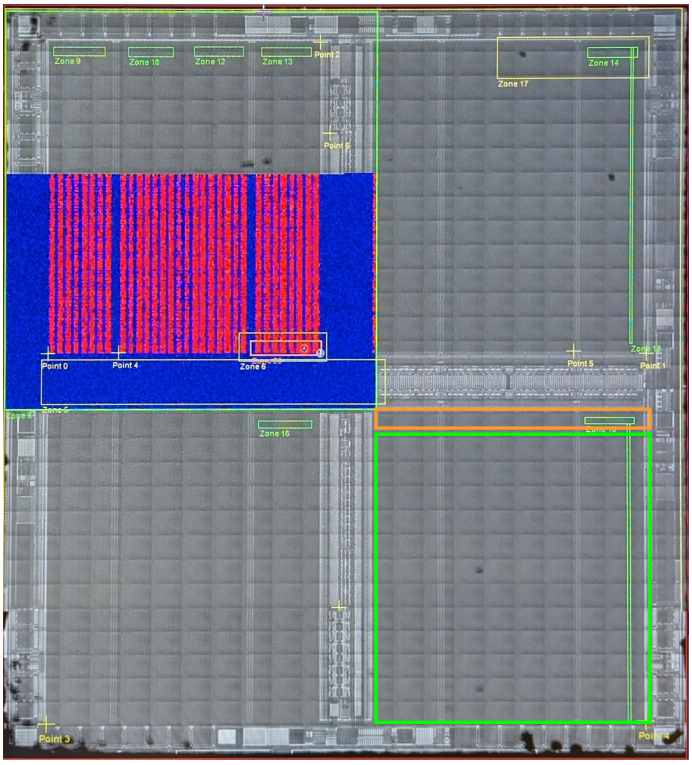

Fig. 7. Laser testing run with chip-enabled test mode of the entire first quadrant, including memory array, supply spines, controlling logic, and periphery interfaces, showing energy and region dependency for SEL occurrence (tested zones highlighted).

orange). It is important to note that the other quadrants had the same behavior. Two Weibulls were fitted from these values, demonstrating a clear distinction of sensitivity in these memory regions. This result suggests region dependency in the SEL sensitivity that could contribute to the findings in the heavy ion characterization, in which lower LETs presented higher cross sections than expected, following a similar trend that could be represented as the combination of the two Weibulls.

Finally, in order to evaluate the impact of the temperature in the laser cross sections, the experiment included testing with different temperatures: $25°C$, $40°C$, $60°C$, and $80°C$. For that, a temperature sensor and a heater were positioned in the DUT for better precision. The heater was placed on the opposing surface of the board for better heating homogeneity, and the sensor was attached to the DUT package, close to the die, for optimal precision but respecting the minimal clearance for the laser. Fig. 9 presents the SEL cross section for the proposed temperature. It is possible to observe a clear correlation between temperature and sensitivity. With higher temperatures, the cross section reaches the asymptotic saturation more rapidly and presents increased sensitivity due to lower energy thresholds (E_{th}).

The complete Weibull parameters are detailed in Table II, including the threshold energy, asymptotic cross section, width, and exponents. As described in [17], an approximated correlation between laser energy and heavy ion LET is possible, but requires a dedicated analysis for refining parameters. The laser equipment used in this experiment provides a first-order approximation of a correlation factor, which yields an equivalent LET value when multiplied by the incident laser energy. For our experiment, the reported factor was approximately 0.086 for a substrate thickness of $300\ \mu m$ (measured by the equipment), providing a rough correlation between the heavy-ion experiment and the laser results.

IV. Flight Analysis

This section presents the flight data collected during the PROBA-V mission and discusses the observed in-flight error rates.

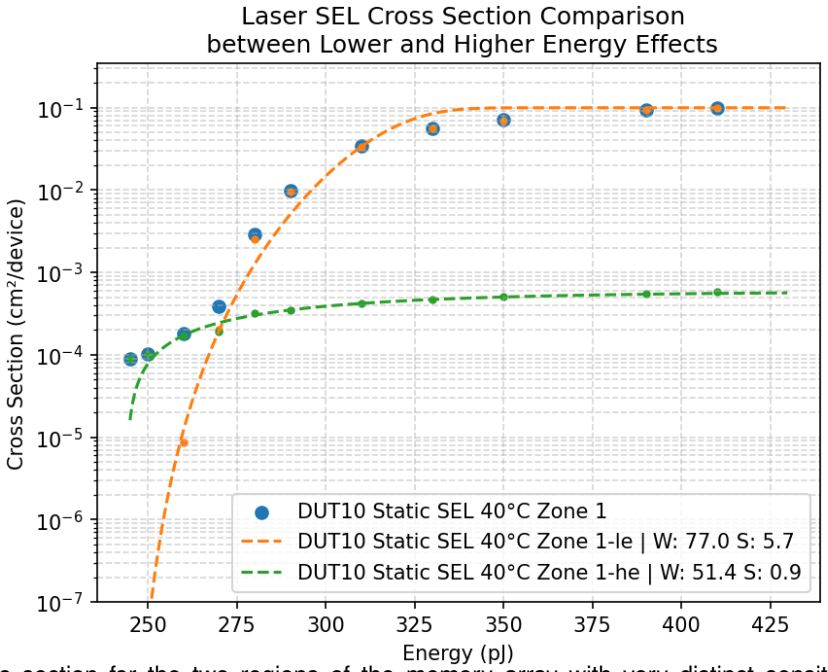

Fig. 8. Static SEL cross section for the two regions of the memory array with very distinct sensitivities. Zone 1-le: $\sigma_{sat} = 5.88 \times 10^{-4}\ cm^2/device$ and $E_{th} = 244\ pJ$. Zone 1-he: $\sigma_{sat} = 9.94 \times 10^{-2}\ cm^2/device$ and $E_{th} = 244\ pJ$.

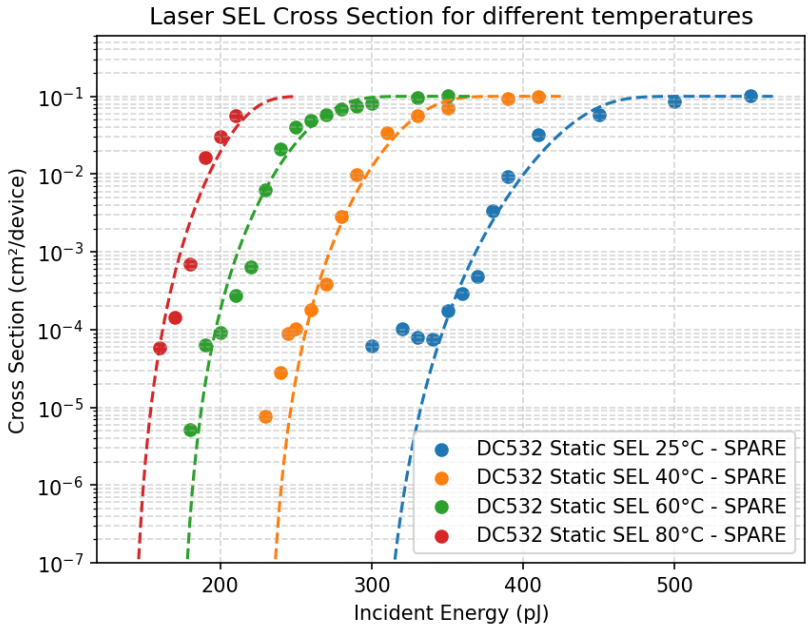

Fig. 9. SEL cross sections for static mode normalized for the entire memory die area using four temperatures: $25°C$, $40°C$, $60°C$, and $80°C$.

A. Flight Data

In order to analyze the log file of all events related to the SRAM memories, we used the Scilab open-source environment. Also, the CelestLab toolbox for Scilab was used to propagate the orbit, perform some mission-related calculations, and plot specific graphs. Regarding estimations for the radiation environment of PROBA-V, we used OMERE tool version 5.3. It was assumed that with protons above $20\ MeV$, a proton particle will likely hit the SRAM memories since their penetration in aluminum is approximately $2.1\ mm$. Hence, our calculations accounted for trapped and solar proton contributions for energies above $20\ MeV$.

TABLE II
WEIBULL PARAMETERS FOR SEL CROSS SECTION USING DIFFERENT TEMPERATURES.

DUT	Temperature [°C]	W	S	E_{th}	σ_{sat}
DUTs 9 and 10	25	145.01	6.28	299.00	0.1
DUT 10	40	104.90	5.19	229.00	0.1
DUT 10	60	100.00	4.98	172.00	0.1
DUT 10	80	80.13	5.35	140.00	0.1

Based on this environment, simplified South Atlantic Anomaly (SAA) and polar regions were defined for the analysis.

Using the CelestLab toolbox, the PROBA-V orbit was propagated, and the average duration passing through the defined regions, as well as the orbital period, were estimated. The results show an orbital period of around 101 minutes, with approximately 10 and 22 minutes over SAA and polar regions, respectively. The algorithm step used for the propagation was 120 seconds, and the orbit was propagated from 8 May 2013 until 18 March 2020. This calculated duration was then used to estimate the average error rates.

Since the launch, on the 7th of May 2013, until the 3rd of March 2020, 1054 events flagged as *type 406* and 77 events flagged as *type 369* have been recorded. Note that *type 369* was not initially used, starting to be registered only later. The first error, *type 406*, occurred on the 8th of May 2013.

Fig. 10 presents the mapping of all reported errors based on the previously defined regions and estimated orbital parameters. As expected, most errors occur either in the SAA or both polar regions. Out of the 1054 errors of flag *type 406*, 868 errors (82.3%) occurred inside the SAA, and 149 errors (14.1%) occurred inside the defined polar regions. Out of the 77 errors of flag *type 369*, the values were, respectively, 69 (almost 89.6%) and 5 (6.4%). 37 errors (approx. 3.5%) are outside both defined zones for flag *type 406* and 3 errors (3.9%) for flag *type 369*. For both types of errors, about 80-90% of errors occur within the SAA regions.

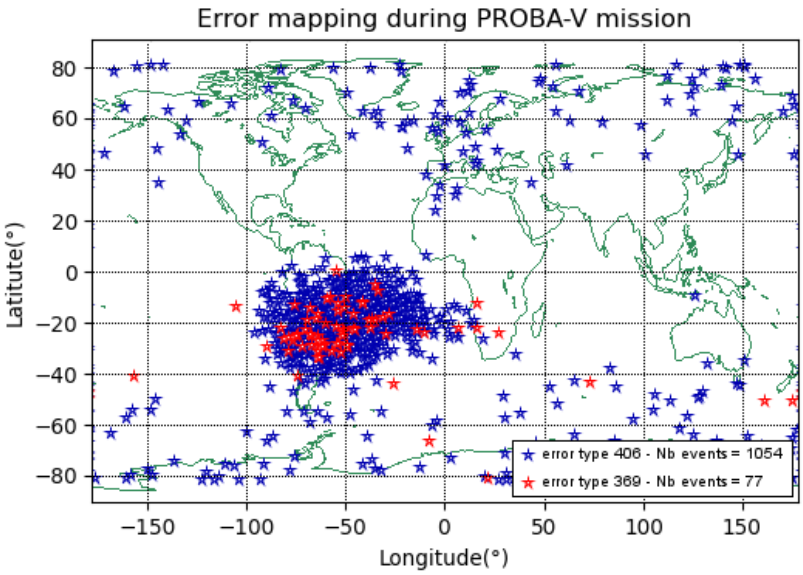

Fig. 10. Mapping of SRAM errors occurring on-board PROBA-V between the 8th May 2013 and the 18th March 2020.

Fig. 11 presents the accumulated errors over a long period of the PROBA-V mission, from which average error rates were observed and estimated. It is possible to conclude that the sensitivity of flag *type 369* errors appears to be much lower than for errors of flag *type 406*, solely looking at the error rate (almost $0.05\ errors/day$ in comparison to close to $0.35\ errors/day$).

Moreover, between April 2016 and May 2017 (days 1062 to 1479), as indicated by vertical lines in the figure, the average error rate was more than two times higher than that experienced before and after

this period. After investigating this behavior with the PROBA-V operators, we found that during this exact period, the MMU lines were reassigned, i.e., the primary was *line 2*, whereas before and after, the primary was *line 1*. Hence, *line 2* indicates a higher sensitivity since the primary line is constantly in use, leaving just a short period of operation for the redundant line during the automatic recovery procedures.

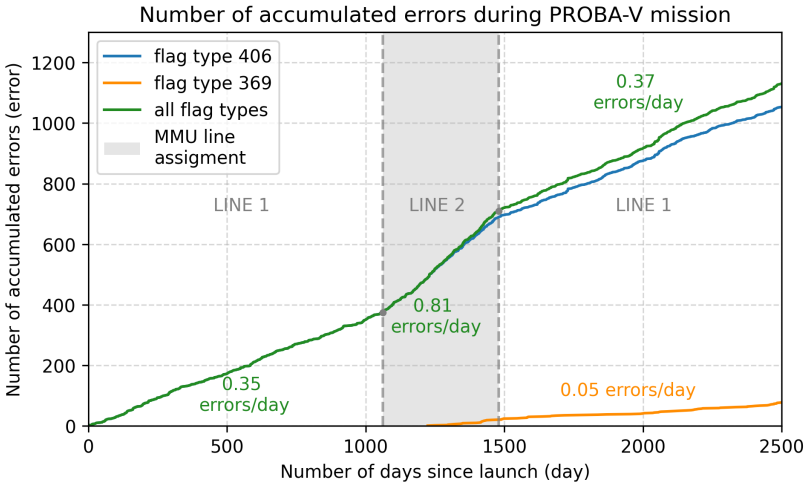

Fig. 11. Accumulative error plot with reference to time occurring on-board the PROBA-V SRAM memories.

B. Rate Estimations with Experimental Data

In order to explore the error rates obtained from the flight flags, we used the acquired experimental data in the OMERE software to estimate the SEL rate according to the PROBA-V orbit. For that, we used similar orbit simulation parameters as described in the previous section. We considered GCRs and trapped particles for the environment, using GCR ISO 15390 (solar activity according to the mission profile) and AP8 (solar minimum) models, respectively. The presented error rate estimations do not consider solar flare activity since none occurred during the analyzed period.

The first hypothesis to describe the in-flight behavior considers that a difference in the equivalent shielding of *line 2* caused the error rate increase since both lines were positioned in distinct regions of the satellite (*line 2* closer to the satellite edges). For that, we ran the estimations considering the entire orbit for different shielding thickness values with the heavy ion and proton data. For the estimated SEL rate, heavy ions were the main contributor. The results for this estimation are presented in the graph shown in Fig. 12. It shows that the equivalent shielding thickness affects the SEL rate, notably for thinner shielding. For instance, a thickness increase from $1.0\ mm$ to $1.5\ mm$ leads to a 33.7% decrease in the SEL rate, whereas from $2.5\ mm$ to $3.0\ mm$, there is a reduction of only 16.5%. Thus, considering an equivalent shielding thickness of a few millimeters for PROBA-V, it is not expected that the shielding alone caused the error rate increase seen while *line 2* was the main line.

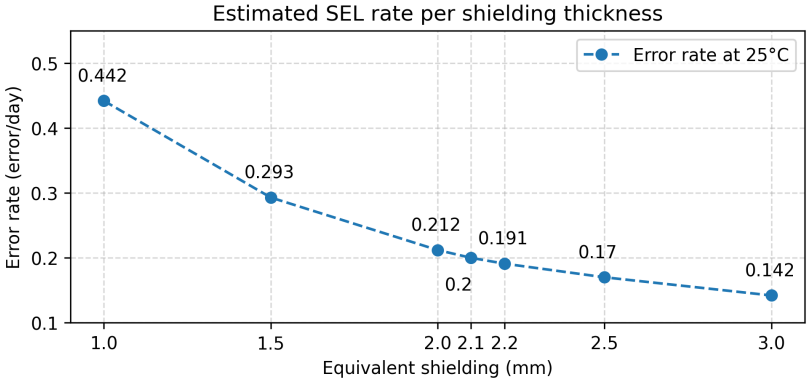

Fig. 12. Estimated in-orbit SEL rate using proton and heavy-ion characterizations with distinct equivalent shielding.

In this context, the second hypothesis proposes that the temperature variation between both lines could also affect the error rate, in which *line 2* would have a higher temperature due to the proximity of *line 2* to the satellite edges. Besides that, during this period, a more intensive operational mode was caused by a change in the scientific payload, which could lead to an overall temperature increase. To investigate this hypothesis, we would need to consider different temperatures for the heavy-ion cross section, which was the main contributor to the SEL rate in orbit. However, we did not include different temperatures for the heavy-ion experiment since our first assumption targeted device variability. Thus, to enable rate estimations, we performed an approximated correlation between the laser testing and the heavy-ion experiment, as shown to be feasible in [17] as a first-order approximation. For that, we compared the characterization at room temperature for both heavy ions and laser, using the correlation factor shown in III-D. This approach provided a rough estimation for the laser cross section concerning LETs, in which the estimated SEL rate for room temperature had a 42% relative error compared with the heavy-ion cross section. In [17], many factors that determine the accuracy of the correlation are presented. Besides these factors, the proposed approximation relies on parameters highly dependent on the device doping and based on modern technologies, which differ from the older device studied in this work. Therefore, for the purpose of relative comparison between different temperatures, the presented estimations are sufficiently representative for assessing the temperature impact hypothesis.

Finally, following this initial estimation, we performed simulations applying the obtained equivalent Weibull curves and acquired the SEL rate for different temperatures with the same shielding parameter of $2.1\ mm$, shown in Fig. 13. We noticed that varying the temperature has an impact on the SEL rate, as expected. With a temperature difference of $20°C$, from $40°C$ to $60°C$, the SEL rate is increased by 79.5%. Hence, the temperature's impact seems to lead to higher SEL rate variations compared to the shielding thickness when considering reasonable values likely experienced during the PROBA-V mission.

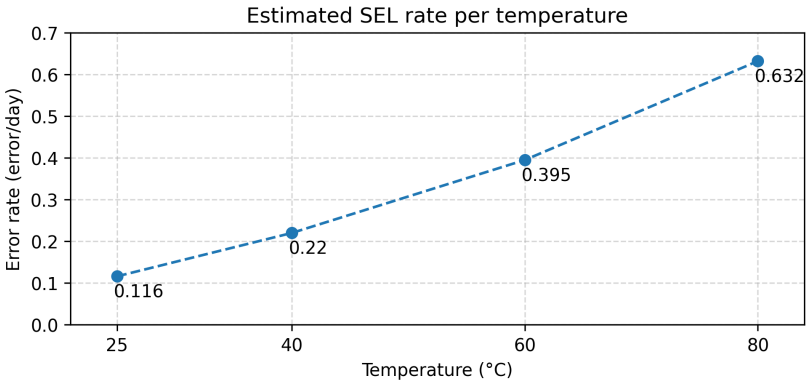

Fig. 13. Estimated in-orbit SEL rate using proton and estimated heavy-ion characterizations with distinct temperatures.

V. Discussion

Similar to the in-flight behavior, the effects identified in the particle accelerator experiments have shown that SELs lead to many upsets in the memory cells. Notably, although the PROBA-V did not monitor the current of the memories in the nominal mode to unequivocally classify SELs, the mission operators noticed this behavior at the beginning of the mission (commissioning), in which more housekeeping data were available, and this correlation could be drawn, allowing the classification of the flag types with the support of the ECC behavior. Hence, with the corroboration of the experimental campaigns' behavior, we can consider a sufficient correlation between flag *type 406* and SELs, as initially assumed.

Regarding the presented cross sections, we observed agreement between devices from the two tested manufacturing lots (*DC532* and *DC419*) and trends similar to Weibull curves. However, with low LET for heavy ions, we observed higher cross sections than expected for the Weibull fitting, which is intriguing since these LET values were not expected to contribute to the error rates significantly and were not even considered for the characterizations prior to the mission. Due to the laser testing campaign, we

were able to investigate this in further detail, and the results suggest an important region dependency for the SEL sensitivity. Besides the previously presented lower and higher energy effects, the internal controlling spines and edge circuitry did not contribute to the SEL cross sections at the tested energies, only the memory array, further highlighting this dependency. Moreover, the laser test campaign enabled the evaluation of the temperature impact on the SEL cross sections by performing an approximate correlation to the experimental heavy-ion data.

Therefore, based on the characteristics of the errors presented in-flight, in this work, we propose the following hypothesis for the observed phenomena. The SRAM devices on-board PROBA-V had similar sensitivities as observed in the experimental analysis, but environmental conditions were different within the satellite, notably temperature and shielding, and this caused the different average rate seen in Fig. 11. In Subsection IV-B, we could observe that reasonable temperature and shielding variations significantly affected the error rate. It is worth mentioning that these modules are not located in the same positions inside the satellite, and the satellite operation modes changed during the mission, so the discussed variation ranges are plausible and expected.

VI. Conclusion

This work presented an analysis of the behavior observed in the PROBA-V SRAM memories, which presented error rate variations in redundant modules that were likely caused by SELs in the devices. To investigate this behavior, we performed experiments in particle accelerator facilities and with laser testing, where we replicated the system characteristics for the accelerated environment to obtain the same phenomenon and analyze the memory with more detailed error information. Moreover, we analyzed the flight data and performed simulations to estimate error rates. The obtained estimations have suggested that temperature and shielding variations were likely responsible for the discernible differences observed when changing the main and redundant lines in the PROBA-V.

Acknowledgment

The authors acknowledge the support given by Etienne Tilmans and René Wittmann from ESA ESEC for having regularly shared the operation log files with the data used in this paper. Also, to Stijn Ilsen and Johan De Hert from QinetiQ for providing background information related to PROBA-V. Finally, to the irradiation facilities personnel that supported the experimental campaigns in this work, including RADEF, PSI, and ESTEC.

References

[1] M. Yang, G. Hua, Y. Feng, and J. Gong, *Fault-tolerance techniques for spacecraft control computers*, 1st ed. John Wiley & Sons, Ltd, Jan. 2017, doi: 10.1002/9781119107392.

[2] E. G. Stassinopoulos and J. P. Raymond, "The space radiation environment for electronics," *Proc. IEEE*, vol. 76, no. 11, pp. 1423–1442, Nov. 1988, doi: 10.1109/5.90113.

[3] S. Bourdarie and M. Xapsos, "The near-earth space radiation environment," *IEEE Trans. Nucl. Sci.*, vol. 55, no. 4, pp. 1810–1832, Aug. 2008, doi: 10.1109/TNS.2008.2001409.

[4] M. Francois, S. Santandrea, K. Mellab, D. Vrancken, and J. Versluys, "The PROBA-V mission: the space segment," *Int. J. Remote Sens.*, vol. 35, no. 7, pp. 2548–2564, Mar. 2014, doi: 10.1080/01431161.2014.883098.

[5] L. Adams, E. Daly, R. Harboe-Sorensen, R. Nickson, J. Haines, W. Schafer, M. Conrad, H. Griech, J. Merkel, T. Schwall, and R. Henneck, "A verified proton induced latch-up in space (CMOS SRAM)," *IEEE Trans. Nucl. Sci.*, vol. 39, no. 6, pp. 1804–1808, Dec. 1992, doi: 10.1109/23.211370.

[6] P. E. Dodd, J. R. Schwank, M. R. Shaneyfelt, V. Ferlet-Cavrois, P. Paillet, J. Baggio, G. L. Hash, J. A. Felix, K. Hirose, and H. Saito, "Heavy ion energy effects in CMOS SRAMs," *IEEE Trans. Nucl. Sci.*, vol. 54, no. 4, pp. 889–893, Aug. 2007, doi: 10.1109/TNS.2007.893425.

[7] G. Bruguier and J.-M. Palau, "Single particle-induced latchup," *IEEE Trans. Nucl. Sci.*, vol. 43, no. 2, pp. 522–532, Apr. 1996, doi: 10.1109/23.490898.

[8] R. D. Schrimpf and D. M. Fleetwood, *Radiation effects and soft errors in integrated circuits and electronic devices*. World Scientific, Jul. 2004, vol. 34, Selected Topics in Electronics and Systems, doi: 10.1142/5607.

[9] *Single Event Effects Test Method and Guidelines*, European Space Components Coordination (ESCC), Std. ESCC Basic Specification No. 25 100, Issue 2, Oct. 2014.

[10] *Space product assurance: Radiation hardness assurance - EEE components*, European Cooperation for Space Standardization (ECSS), Std. ECSS-Q-ST-60-15C, Oct. 2012.

[11] V. Ferlet-Cavrois, “Essentials for electronics in the space radiation environment - test methods and facilities,” in *RADSAGA Final Conference and Industrial Event and RADNEXT Public Kick-Off*. Geneva, Switzerland: CERN, May 2021, [Online] Available: https://indico.cern.ch/event/983095/contributions/4255767/. Accessed on: Feb. 2, 2024.
[12] R. García Alía, M. Brugger, E. Daly, S. Danzeca, V. Ferlet-Cavrois, R. Gaillard, J. Mekki, C. Poivey, and A. Zadeh, “Simplified SEE sensitivity screening for COTS components in space,” *IEEE Trans. Nucl. Sci.*, vol. 64, no. 2, pp. 882–890, Feb. 2017, doi: 10.1109/TNS.2017.2653863.
[13] F. Bezerra, D. Dangla, F. Manni, J. Mekki, D. Standarovski, R. G. Alia, M. Brugger, and S. Danzeca, “Evaluation of an alternative low cost approach for SEE assessment of a SoC,” in *Proc. Eur. Conf. Radiat. Its Eff. Compon. Syst., 17th*, Geneva, Switzerland, 2017, pp. 418–422, doi: 10.1109/RADECS.2017.8696219.
[14] R. Secondo, R. G. Alía, P. Peronnard, M. Brugger, A. Masi, S. Danzeca, A. Merlenghi, J.-R. Vaillé, and L. Dusseau, “Analysis of SEL on commercial SRAM memories and mixed-field characterization of a latchup detection circuit for LEO space applications,” *IEEE Trans. Nucl. Sci.*, vol. 64, no. 8, pp. 2107–2114, Aug. 2017, doi: 10.1109/TNS.2017.2691403.
[15] N. Kerboub, R. G. Alia, J. Mekki, F. Bezerra, A. Monteuuis, P. Fernández-Martinez, S. Danzeca, M. Brugger, D. Standarovski, and J. Rauch, “Comparison between in-flight SEL measurement and ground estimation using different facilities,” *IEEE Trans. Nucl. Sci.*, vol. 66, no. 7, pp. 1541–1547, Jul. 2019, doi: 10.1109/TNS.2019.2915019.
[16] D. V. Savchenkov, A. I. Chumakov, A. G. Petrov, A. A. Pechenkin, A. N. Egorov, O. B. Mavritskiy, and A. V. Yanenko, “Study of SEL and SEU in SRAM using different laser techniques,” in *Proc. Eur. Conf. Radiat. Its Eff. Compon. Syst., 14th*, Oxford, United Kingdom, Sept. 2013, pp. 430–434, doi: 10.1109/RADECS.2013.6937411.
[17] *Single-Event Effects Testing with a Laser Beam - Guidelines*, Institute of Electronics and Systems (IES), European Space Agency (ESA), Std. ESA-TN2, Rev. TN2, May 2022.
[18] J. Budroweit and H. Patscheider, “Risk assessment for the use of COTS devices in space systems under consideration of radiation effects,” *Electronics*, vol. 10, no. 9, Apr. 2021, Art. no. 1008, doi: 10.3390/electronics10091008.
[19] R. Harboe-Sorensen, C. Poivey, F.-X. Guerre, A. Roseng, F. Lochon, G. Berger, W. Hajdas, A. Virtanen, H. Kettunen, and S. Duzellier, “From the reference SEU monitor to the technology demonstration module on-board PROBA-II,” *IEEE Trans. Nucl. Sci.*, vol. 55, no. 6, pp. 3082–3087, Dec. 2008, doi: 10.1109/TNS.2008.2006896.
[20] R. Harboe-Sorensen, C. Poivey, A. Zadeh, A. Keating, N. Fleurinck, K. Puimege, F.-X. Guerre, F. Lochon, M. Kaddour, L. Li, and D. Walter, “PROBA-II technology demonstration module in-flight data analysis,” *IEEE Trans. Nucl. Sci.*, vol. 59, no. 4, pp. 1086–1091, Aug. 2012, doi: 10.1109/TNS.2012.2185062.
[21] M. D’Alessio, C. Poivey, V. Ferlet-Cavrois, H. Evans, R. Harboe-Sørensen, A. Keating, I. Lopez-Calle, F. X. Guerre *et al.*, “SRAMs SEL and SEU in-flight data from PROBA-II spacecraft,” in *Proc. Eur. Conf. Radiat. Its Eff. Compon. Syst., 14th*, Oxford, United Kingdom, Sept. 2013, pp. 91–98, doi: 10.1109/RADECS.2013.6937398.
[22] *256K x 16 Bit High-Speed CMOS Static RAM*, Samsung. K6R4016V1D Datasheet, 2004, rev. 4.0.
[23] *Single Event Effects - A Comparison of Configuration Upsets and Data Upsets*, Microsemi Corporation. WP0203 White Paper, 2015, rev. 1. [Online] Available: https://www.microsemi.com/document-portal/doc_view/135837-wp0203-single-event-effects-a-comparison-of-configuration-upsets-and-data-upsets. Accessed on: Feb. 2, 2024.
[24] L. Dilillo, G. Tsiligiannis, V. Gupta, A. Bosser, F. Saigne, and F. Wrobel, “Soft errors in commercial off-the-shelf static random access memories,” *Semicond. Sci. Technol.*, vol. 32, no. 1, Dec. 2016, Art. no. 013006, doi: 10.1088/1361-6641/32/1/013006.
[25] G. Tsiligiannis, L. Dilillo, A. Bosio, P. Girard, A. Todri, A. Virazel, A. D. Touboul, F. Wrobel, and F. Saigné, “Evaluation of test algorithms stress effect on srams under neutron radiation,” in *Proc. Int. On-Line Test. Symp., 18th*, Sitges, Spain, June 2012, pp. 121–122, doi: 10.1109/IOLTS.2012.6313853.
[26] P. E. Dodd, J. R. Schwank, M. R. Shaneyfelt, J. A. Felix, P. Paillet, V. Ferlet-Cavrois, J. Baggio, R. A. Reed *et al.*, “Impact of heavy ion energy and nuclear interactions on single-event upset and latchup in integrated circuits,” *IEEE Trans. Nucl. Sci.*, vol. 54, no. 6, pp. 2303–2311, Dec. 2007, doi: 10.1109/TNS.2007.909844.
[27] V. Ferlet-Cavrois, J. R. Schwank, S. Liu, M. Muschitiello, T. Beutier, A. Javanainen, A. Hedlund, C. Poivey *et al.*, “Influence of beam conditions and energy for SEE testing,” *IEEE Trans. Nucl. Sci.*, vol. 59, no. 4, pp. 1149–1160, Apr. 2012, doi: 10.1109/TNS.2012.2187681.
[28] A. Coronetti, R. G. Alìa, J. Wang, M. Tali, M. Cecchetto, C. Cazzaniga, A. Javanainen, F. Saigné, and P. Leroux, “Assessment of proton direct ionization for the radiation hardness assurance of deep submicron srams used in space applications,” *IEEE Trans. Nucl. Sci.*, vol. 68, no. 5, pp. 937–948, Feb. 2021, doi: 10.1109/TNS.2021.3061209.
[29] N. A. Dodds, M. J. Martinez, P. E. Dodd, M. R. Shaneyfelt, F. W. Sexton, J. D. Black, D. S. Lee, S. E. Swanson *et al.*, “The contribution of low-energy protons to the total on-orbit SEU rate,” *IEEE Trans. Nucl. Sci.*, vol. 62, no. 6, pp. 2440–2451, Dec. 2015, doi: 10.1109/TNS.2015.2486763.
[30] S. Buchner, P. Marshall, S. Kniffin, and K. LaBel, *Proton Test Guideline Development – Lessons Learned*, NASA/Goddard Space Flight Center, NEPP, Aug. 2002, [Online] Available: https://radhome.gsfc.nasa.gov/radhome/papers/proton_testing_guidelines _2002.pdf. Accessed on: Feb. 6, 2024.